CORA Cork Open Research Archive
Cartlann Taighde Oscailte Chorcaí

Title	Embedding colloidal nanoparticles inside mesoporous silica using gas expanded liquids for high loading recyclable catalysts
Authors	Collins, Gillian;Rahme, Kamil;O'Connell, John;Holmes, Justin D.
Publication date	2016-07-11
Original Citation	Collins, G., Rahme, K., O'Connell, J., and Holmes, Justin D. (2016) 'Embedding colloidal nanoparticles inside mesoporous silica using gas expanded liquids for high loading recyclable catalysts', Catalysis Science and Technology, 6(19), pp 7212-7219. doi: 10.1039/C6CY00584E
Type of publication	Article (peer-reviewed)
Link to publisher's version	10.1039/C6CY00584E
Rights	© 2016, The Authors. Reproduced from Catalysis Science & Technology with permission from the Royal Society of Chemistry.
Download date	2026-11-06 01:13:08
Item downloaded from	https://hdl.handle.net/10468/3141

UCC
University College Cork, Ireland
Coláiste na hOllscoile Corcaigh

Journal Name

ARTICLE

Embedding Colloidal Alloy Nanoparticles in SBA-15 by Supercritical Fluids for High Loading Recyclable Catalysts

G. Collins[a, b,*], K. Rahme[a,c], J. O'Connell[a,b] and J. D. Holmes[a, b]

Received 00th January 20xx,
Accepted 00th January 20xx

DOI: 10.1039/x0xx00000x

www.rsc.org/

The ability to tune the structural and chemical properties of colloidal nanoparticles (NPs), make them highly advantageous for studying activity and selectivity dependent catalytic behaviour. Incorporating pre-synthesized colloidal NPs into porous supports materials remains a challenge due to poor wetting and pore permeability. In this report monodisperse, composition controlled AgPd alloy NPs were synthesised and embedded into SBA-15 using supercritical carbon dioxide and hexane. Supercritical fluid impregnation resulted in high metal loading without the requirement for surface pre-treatments. The catalytic activity, reaction profiles and recyclability of the alloy NPs embedded in SBA-15 and immobilised on non-porous SiO_2 are evaluated. The NPs incorporated within the SBA-15 porous network showed significantly greater recyclability performance compared to non-porous SiO_2.

Introduction

Colloidal nanoparticles (NPs) for catalytic applications are becoming more complex with parameters such as size, shape, chemical composition and crystallinity playing a central role in optimising catalytic performance. The application of bimetallic NPs including alloys and core-shell structures are gaining interest due to their enhanced activity or selectivity.[1, 2] Continuing developments in colloidal synthesis is enabling greater control of structural and chemical features at the nanoscale. The majority of catalytic applications requires immobilisation of colloidal NPs onto support materials, with activated carbon or nonporous oxide supports most commonly used for pre-synthesized NPs, however incorporation of NPs into porous supports is desirable. The main advantages of using ordered mesoporous solids in catalysis are the relatively large pores (~2-50 nm) which facilitate mass transfer and the very high surface area which allows a high concentration of active sites per mass of material. Furthermore, embedding NPs into porous networks can increase catalyst stability and limit loss of the active metal during reaction conditions.[3]

Mesoporous silica materials offer board structural diversity in terms of both pore architecture and dimensions, making them versatile as catalyst support materials.[4] The preparation of NP-mesoporous materials is typically based on incipient wetness (IW) impregnation methods, which involves mixing the support with a metal precursor solution, usually a salt, followed by reduction to yield metallic NPs.[4] While this is a facile and general method, it is characterised by several drawbacks. Surface functionalisation of the silica to introduce functional groups such as amines or thiols are often needed to bind the metal precursor to obtain reasonable metal loadings.[5] A considerable disadvantage is the inability to finely control the structural and chemical properties of the NPs. As catalytic activity and selectivity is highly sensitive to these parameters, IW impregnation methods also limit the study of structure-property relationships in catalysis. In contrast to IW-impregnation methods, pre-synthesised colloidal NPs prepared through wet-chemical methods allow for exceptional control over the chemical and physical properties of NPs. Immobilisation of colloidal NPs into mesoporous supports presents several challenges. The relatively high surface tension and viscosity in most liquid solvents hinders wetting of the support surface limiting diffusion of NPs into the pores, therefore leading to formation of poorly dispersed NPs with a non-homogeneous distribution and low metal loading. Recent experiments involving single-particle tracking through three-dimensional porous polymers showed significant hydrodynamic damping of particle motion and illustrated that volume accessibility is more limited than previously expected.[6]

Several strategies have been developed to incorporate colloidal NPs into porous materials. One approach has been the use of hierarchical porous supports which are characterised by porosity on multiple scale lengths.[7] In such systems the larger pores allow penetration into the porous matrix while the small pores maintain high surface area. Another approach has been to grow a porous oxide shell around the colloidal NPs creating a support-NP core-sell structure, but agglomeration and ordering

[a] Department of Chemistry and the Tyndall National Institute, University College Cork, Cork, Ireland.
[b] CRANN@AMBER, Trinity College Dublin, Dublin, Ireland.
[c] Address here Kamil. Email g.collins@ucc.ie
† Footnotes relating to the title and/or authors should appear here.
Electronic Supplementary Information (ESI) available: [details of any supplementary information available should be included here]. See DOI: 10.1039/x0xx00000x

Please do not adjust margins

of the pore structure are difficult to control.[8, 9] More recently, attempts to make an interconnected mesoporous TiO_2 support around colloidal Au NPs using organic spacers to tune the porosity of the support, also proved effective.[10] Incorporation of colloidal NPs into highly ordered porous oxides is still desirable. In this study we use a direct method of impregnating colloidal NPs onto a SBA-15 support using supercritical fluids. A supercritical fluid is defined as a single phase which occurs when a substance is held above its critical temperature and pressure.[11] SCFs provide a unique reaction medium with density tuneable solvation properties, and are typically characterised by low gas-like viscosities, high diffusion coefficients and no surface tension. These unique properties of SCFs have found many applications including the synthesis of nanostructures, coatings, sol-gels and extraction/drying processes.[12, 13] The increased pore permeability make SCFs an ideal media for impregnation into porous materials. The most common approach for preparing NP supported catalysts is dissolving the metal precursor in the SCF (usually CO_2) for impregnation, followed by decomposition or reduction of the precursor to give well dispersed NPs. Unlike conventional liquid-phase impregnation, the high diffusivity and zero surface tension of SCFs allows for increased precursor penetration and wetting of the pores and high metals loadings can be achieved without the need for pre-treatments like surface modification.[14] Despite the use of SCFs for NP synthesis and processing, SCFs are not commonly used for impregnation pre-synthesized colloidal NPs, which is mainly attributed to the weak solvating power of many SCFs.[15] In this study we show that a mixture of hexane and sc-CO_2 can be used to effectively impregnate organically capped NPs into SBA-15 support without the need for surface pre-treatment. Importantly, SCFs are effective for embedding NPs with diameters comparable to that of the support pore diameter. The catalytic performance is assessed and compared with NPs immobilised on non-porous SiO_2 supports in Suzuki cross coupling reactions, which is a well-known reaction for inducing metal dissolution. Pore incorporation does not hinder catalytic activity and embedding the NPs within a porous support significantly improves catalyst recyclability.

Experimental

Materials and methods

Preparation of AgPd NPs was prepared using a modified procedure previously described.[16] Briefly, Ag seed NPs were first prepared by heating a solution containing 90 mg of $AgNO_3$ in 20 mL of oleylamine to 160 °C in an Ar atmosphere under magnetic stirring for 1 h. For the synthesis of AgPd alloy NPs, 60 mg of $PdCl_2$ was immediately added to the above Ag seed solution, and the mixture was heated at 220 °C for 1 h under Ar atmosphere and rapid magnetic stirring. The solution as cooled to room temperature and ethanol was added to precipitate the NPs, which were collected by centrifuge at 8000 rpm for 15 min. The supernatant was discarded and the NPs were redispersed in a minimum amount of toluene and sonicated briefly. Ethanol was again added to precipitate the NPs which were collected by centrifuge. This cleaning procedure was repeated three times. Short channel SBA-15 was prepared by a method described by Zhang and co-workers.[16] Briefly, 2.4 g of EO20PO70EO20 (P123) was dissolved in 84 ml of 1.07 M HCl solution and stirred at room temperature until dissolved. Decane (19 ml) was added to the solution. The mixture was stirred at room temperature for 1 h. Finally, 0.027 g of NH_4F was added under stirring as a hydrolysis catalyst, followed by 5.1 g of tetraethyl orthosilicate (TEOS). The mixture was stirred at 40 °C for 20 h and then transferred into an autoclave for further reaction at 100 °C for 48 h. The products were collected by filtration, dried in air, and calcined at 550 °C for 5 h to remove the templates.
Incorporation of NPs into SBA-15 was carried out by supercritical (sc) fluid inclusion. The SBA-15 support and NPs dispersed in hexane were briefly sonicated to disperse the SiO_2 and then added to a 5 ml high pressure stainless steel vessel. The vessel was heated to 180 °C and pressurized to 10.3 MPa by sc-CO_2 and held for 20 min, after which time the vessel was slowly depressurized. The catalyst was washed with hexane and dried. Finally, to remove any residual oleylamine capping ligands and promote adhesion of the NPs to the SiO_2 surface, the catalysts were annealed at 200 °C for 5 h in air.

Materials Characterization

Scanning electron microscopy (SEM) images were obtained using a FEI DualBeam Helios NanoLab 600i high resolution SEM equipped with an Oxford Instruments AZTec system with X-Max 80 detector. Transmission electron microscopy (TEM) analysis was performed using a Joel 2100 electron microscope at an operating voltage of 200 kV. XPS spectra were acquired on an Oxford Applied Research Escabase XPS system. A non-monochromated Al-kα x-ray source at 200 W power was used for all scans. Pd 3d core level scans were acquired at the applicable binding energy range, with a step size of 0.1 eV, dwell time of 0.05 s and pass energy of 20 eV averaged over 100 scans. Spectra were charge corrected with respect to the C 1s at 285 eV. Data was processed using CasaXPS software where a Shirley background correction was employed and peaks were fitted to Voigt profiles.

Catalytic Characterization

In a typical reaction, 2.2 mmol of phenylboronic acid 2 mmol of aryl halide and 2 equivalents of K_2CO_3 were added a 3:1 ethanol/water solvent. The reactions were carried out at room temperature and were initiated by addition of the catalyst. Reactions were sampled at regular intervals for GC analysis. Samples were analyzed using an Agilent 7890A GC system, equip with a flame ionization detector (FID). Products were identified against authenticated standards and quantified by calibration to obtain response factors (RF) against the known internal standard (dodecane). For calculation of the surface normalized turn over frequency (TOF), the number of atoms (N_{Tot}) in a NP was estimated based on formula by Benfield for NPs with a icosahedral geometry.[17] The total number of atoms in a NPs with an edge length of a, $(N_{Tot}) = ⅓(2m - 1)(5m^2 - 5m + 3)$, where m is the number of atoms along the edge length. The edge length was calculated from basic geometry using the mean NP diameter determined from TEM *i.e.* for NPs of a mean diameter of 8 nm, a =

 This journal is © The Royal Society of Chemistry 20xx

Please do not adjust margins

Please do not adjust margins

4.2 nm. The total number of surface atoms, N_{Surf}, in a NPs was calculated using $N_{Surf} = 10m^2 - 20m + 12$. Therefore, the percentage of surface atoms was estimated by $N_{Surf}/N_{Tot} \times 100$. For the recyclability tests, the reaction scale was increased to 8 mmol of the aryl halide. After the reaction, dichloromethane was added to the reaction mixture to extract the reaction product. The organic layer was discarded and the catalyst was recovered by centrifugation. The catalyst was washed in ethanol and water and re-weighed.

Results and discussion

Nanoparticle Synthesis and Immobilisation

AgPd NPs were chosen as a model colloidal system for the study due to their various catalytic and electrocatalytic applications. PdAg alloys display exceptionally high activity and CO tolerance in dehydrogenation of formic acid.[18] Bimetallic PdAg systems are widely used as selective hydrogenation catalysts.[19-21] Recently, AgPd NPs have been used for selective methylation of aromatic amines[22]. Ag alloys facilitates light driven catalytic behaviour which has been demonstrated in hydrogenation of styrene.[23] Figure 1 (a) shows a TEM image of the AgPd NPs prepared by displacement reaction of Ag NPs in oleylamine at 220 °C. Addition of the Pd(II) salt to the Ag NP solution results in rapid interdiffusion of Pd atoms into Ag NPs and the formation of AgPd alloys.[24, 25] The resultant NPs are multiply twinned as shown in the high resolution TEM image in Figure 1 (b), where the NP is orientated on its 5-fold symmetry, possessing a icosahedral morphology. Multiply twinned NPs are characterized by a high density of interfacial vacancy defects along the NP grain boundaries, which are often beneficial to catalytic activity.[24] The mean diameter and diameter distribution shown in Supporting Information Figure S1 shows the average NP diameter is 8 nm (standard deviation = 1.26). EDX analysis confirms that the particles are alloys with a SBA-

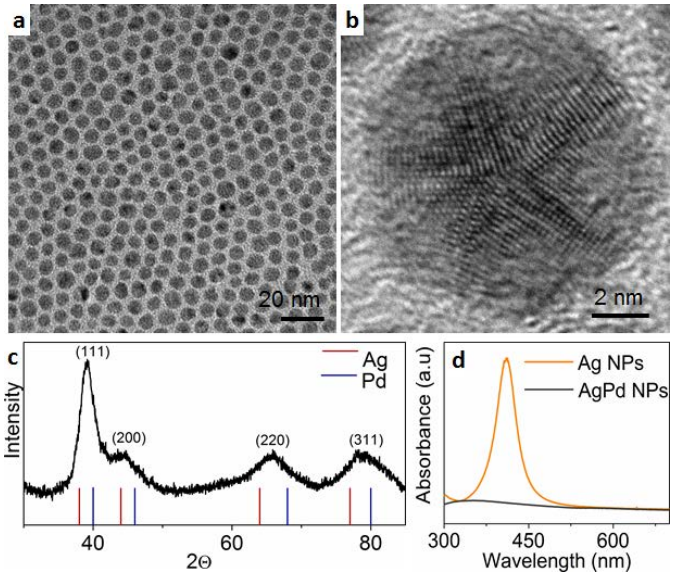


Figure 1. TEM image of (a) AgPd NPs. (b) High resolution TEM of single AgPd NP showing multiple twinned structure. (c) XRD pattern of AgPd NPs. (d) UV-vis spectrum of the Ag NPs and after addition of Pd precursor resulting in extinction of the LSPR.

15, which is a mesoporous silica with uniform pore structure and high surface area was chosen as the model support material. Short channel SBA-15 with a cuboid morphology and the pore channel of 200 nm in length, as shown in Figure 2(a) was used instead of conventional SBA-15, which is characterized by longer pore channels.[16] The benefit of using straight, short channel SBA-15 supports is improved mass transfer in liquid phase reactions.[3] A further objective of the study was to evaluate the immobilisation of NPs with a comparable diameter to that of the porous support. The pore channels of the SBA-15 measured by HRTEM were 10.5 nm in diameter (Supporting Information Figure S3), which are comparable with but large enough to accommodate the pre-synthesized colloidal NPs (8 nmomposition of $Ag_{0.65}Pd_{0.34}$ (Supporting information, Figure S2). The XRD pattern of the alloy NPs, shown in Figure 1 (c) displays a pattern similar to that of face centred cubic Pd and Ag. The diffraction pattern consists of broad overlaying peaks, which can be assigned to the (111), (200), (220) and (311) peaks of Pd at 39°, 46°, 68° and 80° and Ag at 38°, 44°, 64°, and 77°.[26] Formation of the alloy composition resulted in significant changes to the optical properties of the Ag seeds with complete extinction of the Ag LSPR at 400 nm, as shown in Figure 1 (d).

NP dispersibility in a solvent requires favourable solvent-ligand interaction to provide sufficient repulsive forces to overcome the strong attractive van der Waals forces between the metallic NPs. Before immobilisation into the support, the solubility of the NPs in SCFs was visually assessed through a sapphire window in a high pressure cell. Kuwahara *et. al.* [27] used sc-CO_2 to embed dodecanethiol capped Au and CdS NPs in porous poly(ethylene terephthalate) (PET) polymer films. The oleylamine capped NPs were not soluble in sc-CO_2, even at pressures high as 34.5 MPa, the increased solvent density was insufficient to solvate the NPs. The poor dispersibility of the NPs is attributed to the weak solvating power of CO_2 and as the strength of the attractive van der Waals forces increases with NP size the use of sc-CO_2 alone could not adequately disperse the 8 nm NPs. Dodecanethiol capped NPs have been reported to be soluble in supercritical alkanes and octanol, therefore the hexane was chosen as the solvent media.[15] The NPs could be dispersed in hexane pressurised with sc-CO_2. Figure 2(b) shows the SBA-15 after impregnation with AgPd NPs.[28] A high density of NPs are observed in the TEM image in Figure 2 (b) and the inset TEM image shows the NPs embedded within the pores of SBA-15. EDX confirms the metal loading of 17.3 wt%. As a control sample to compare the effectiveness of embedding NPs using SCFs, the NPs dissolved in hexane, were sonicated for 30 mins in the presence of SBA-15. Figure 2(c) shows a typical TEM image after sonication. While some pore filling was observed low NP incorporation into the pores was readily apparent by TEM. Furthermore, NP dispersion was poor and the NP density was highest at the entrance to the pores. The lower NP loading obtained through sonication were also verified by EDX analysis showing a metal loading of 3.2 wt%. The high degree of pore filling under supercritical fluid conditions is further indicated by the BET analysis of the catalysis, shown in Figure 2 (d). BET analysis of the blank SBA-15 confirms a high surface area of 789

Please do not adjust margins

Please do not adjust margins

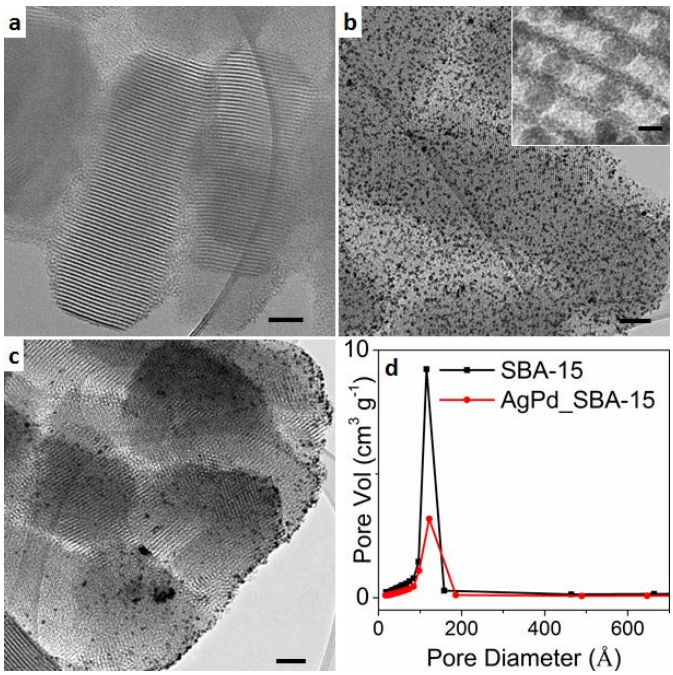


Figure 2. TEM image of (a) short channel SBA-15. (b) After supercritical fluid impregnation with AgPd NPs. (c) After sonication of SBA-15 in AgPd NP solution for 30 min. (d) BET analysis of SBA-15 before and after NP impregnation. The scale bars in (a)-(c) are 100 nm, scale bar in figure (b) inset is 5 nm.

m^2g^{-1} with a pore volume and pore diameter of 1.7 $cm^3\,g^{-1}$ and 11 nm, respectively. After NP inclusion, the surface area and pore volume decreased to 346 m^2g^{-1} and 0.86 $cm^3\,g^{-1}$ respectively, consistent with incorporation of NPs into the porous matrix. A slight increase is observed in the pore diameter as can be seen Figure 2 (d), which is attributed to pore swelling by under supercritical fluids.

Catalytic Evaluation

The catalytic activity of the alloy supported NPs were tested in Suzuki cross coupling which is an important reaction in the construction of biaryl fragments and is widely used in organic synthesis and pharmaceutical fields.[29] Leaching processes are well-associated with NP catalysed Suzuki coupling reactions and can lead to lower activity and loss of catalyst recyclability due to dissolution of the active metal and aggregation of NPs.[30, 31] While the Suzuki reaction can be efficiency catalysed under homogeneous conditions, a key motivator for the use of heterogeneous catalysts is the potential to recycle the catalyst. Therefore improving the durability and stability of the NPs through embedding them within a porous support is highly advantageous**.** Alloy NPs have shown superior activity in a range of coupling reactions**.** AuPd alloys have been used for visible light enhanced Suzuki, Heck, Stille and Sonogashira coupling.[32] PdNi alloys displayed better activity, selectivity and stability in Heck coupling.[33] Highly dilute AuPd alloys are effective for single atom Ullmann coupling of aryl chlorides in water.[34]

To evaluate the use of porous SBA-15 support material for Suzuki coupling, a non-porous catalyst was prepared by immobilising the AgPd alloy NPs onto nano-powdered non-porous SiO_2 powder, as shown in the TEM image in Supporting Information Figure S4. The surface area of the SiO_2 determined by BET analysis was 5.1 $m^2\,g^{-1}$ and the catalyst metal loading was 2.6 wt.% (0.91 wt.% equivalent Pd). The catalytic performance of the NPs immobilised on the two support materials was compared by evaluating the reaction profiles in the cross coupling of phenylboronic acid and iodo- or bromobenzene. The reaction profiles of the SBA-15 and non-porous SiO_2 are illustrated in Figure 3 (a). For the cross coupling of iodobenzene both the SBA-15 and non-porous catalysts displayed similar profiles. No induction period was observed and the reaction was catalysed to completion. Greater differences in the reactivity trend for the two support materials was observed for the cross coupling of bromobenzene. While both reactions showed an induction period, the reaction was initiated faster with the non-porous SiO_2 catalyst, with conversion at 12% after 30 min, while no biaryl product was detected with the SBA-15. However, as the reaction progressed, conversion with the non-porous catalyst slowed giving a yield of 51% after 420 min, compared to 67% for the SBA-15 supported NPs. Importantly, even though the Pd sites were embedded in the pores of the SBA-15 support, the mass transfer of the reagents and products were not inhibited due to the limited space or poor wettability.

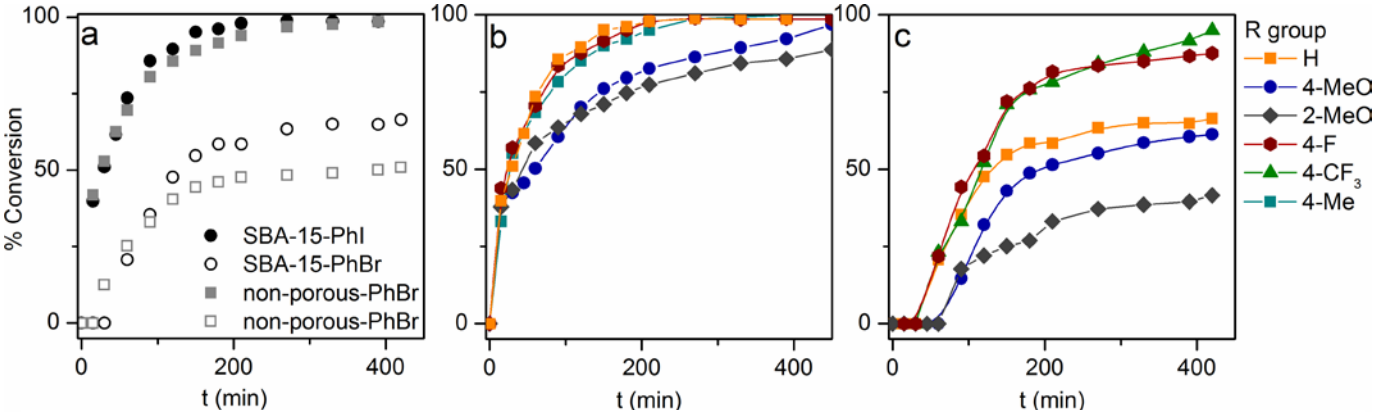
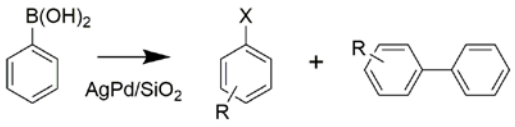


Figure 3. (a) Reaction profile of Suzuki coupling comparing NPs immobilised on SBA-15 and non-porous SiO_2. (b) Reaction profiles of Suzuki cross coupling of phenylboronic acid and aryl iodides. (c) Reaction profiles of Suzuki cross coupling of phenylboronic acid and aryl bromides.

This journal is © The Royal Society of Chemistry 20xx

Please do not adjust margins

Table 1. Catalytic performance of AgPd NPS on SBA-15.



Ar-X	R	% Yield [a]	TON Abs [b]	TON surf [c]	TOF surf h-1[c]
Ph-I	H	99	1131	5955	999
Ph-I	Me	97	1109	5835	973
Ph-I	4-MeO	99	1131	5995	999
Ph-I	2-MeO	89	1017	5353	892
Ph-I	4-F	99	1131	5955	999
Ph-Br	H	58	663	3488	460
Ph-Br	4-MeO	61	697	3669	489
Ph-Br	4-MeO	95[d]	1086	5714	238
Ph-Br	4-MeO	98[e]	1120	5895	786
Ph-Br	2-MeO	42	480	2526	337
Ph-Br	4-F	86	983	5173	690
Ph-Br	4-CF_3	92	1051	5534	738

Conditions: aryl halide (2 mmol), phenylboronic acid (2.2 mmol), K_2CO_3 (2 equivalents), EtOH:H_2O (2:1), 0.5 mol% AgPd which is equivalent to 0.175 mol% Pd. Reaction carried out at room temperature (~20 °C). [a] GC yield with dodecane as internal standard. [b] TON = mol of aryl halide converted/ mol Pd. [c] TOF_{surf} = mol converted aryl halide/ mol surface Pd h^{-1}. TOF_{surf} for aryl iodide halide calculated after 6 h. TOF_{surf} for aryl bromide calculated after 7.5 h. [d] Yield after 24 h. [d] Reaction temperature of 60 °C.

The reactivity of AgPd-SBA-15 catalysts in Suzuki reaction was further investigated to evaluate the influence of the aryl halide substituents. Figure 3 (a) and (b) compares the reaction profiles of aryl iodides and bromides with different ring substituent groups. Table 1 summarises the absolute TONs based on the Pd mass and the surface normalised TONs and TOFs. Coupling of aryl iodides proceeded quickly with no induction period observed. Unactivated and sterically hindered aryl iodides showed marginally lower conversions compared to activated aryl iodides but the initial rate profiles for all aryl iodides was identical and excellent reaction yield of 89-99% were observed at room temperature. The surface normalised TOFs for aryl iodides ranged from 892-999 h^{-1}. In contrast to the aryl iodides, all the aryl bromides tested displayed an induction period, varying from 30-60 min and were more sensitive to electronic and steric effects of the aryl bromide. Deactivated aryl bromides had longer induction periods and lower conversions than activated bromides as shown in Figure 3 (c). The lower activity of the aryl bromides is expected due to great C-Br bond strength. Increasing the reaction time or temperature to 60 °C resulted in yields of 95 and 98% for 4-methoxybenzene, as shown in Table 1. No competing homocoupling of the boronic acid or aryl halide was observed with the desired cross coupled biaryl the only reaction product.

One of the major benefits of heterogeneous catalysts is the potential to recover and reuse the catalyst after the reaction. The catalytic recyclability of AgPd NPs was studied using iodotoluene and phenylboronic acid as the model reaction. Figure 4 (a) compares the conversion observed for AgPd NPs supported on SBA-15 and non-porous SiO_2 over 4 reaction recycles. On the first reaction cycle both catalyst supports performed well, catalysing the reaction to completion after 3.5 h. The SBA-15 and non-porous supports display significantly different recyclability performance. The NPs immobilised on the SBA-15 displayed good recyclability with yields of 92%, 85% and 80% in the 2nd, 3rd and 4th reaction cycles, respectively. TEM analysis of the catalyst after the reactions showed some evidence of NP broadening but good NP dispersion was maintained as illustrated in the TEM image in Fig. 4 (b). The mean diameter and standard deviation of the NPs increased from 8 nm (std. dev. = 1.26) to 8.4 nm (std. dev. = 2.63) as shown in the distribution histogram in Supporting Information Fig. S5. In contrast to the NPs supported on SBA-15, the NPs immobilised on non-porous SiO_2 displayed very poor recyclability. The yield decreased to 22% in the second reaction cycle and only trace amounts of the reaction product was observed by reaction cycle 4. Leaching and dissolution process are well-known to occur in the Suzuki reaction with the aryl halide, boronic acid, base and solvent all demonstrated to induce loss of Pd.[30, 35] The dramatic difference between the two catalyst indicates the important of the support architecture and NP-support interactions. EDX analysis showed a 34% decrease in Pd concentration in the non-porous SiO_2 after the first cycle. TEM analysis of the reaction supernatant catalysed using the non-porous SiO_2, also showed the presence of NPs which had be removed from SiO_2 (Supporting Information Figure S6.) The loss of recyclability originates mainly from poor adhesion of the NPs to the SiO_2 support. The low and gradual loss in activity observed for the SBA-15 catalyst is likely attributed to low level dissolution of Pd, which is typically reported to be in the order of a few parts per million for aqueous solutions.[36]

The Pd 3d core level spectra of the fresh and used catalyst is shown in Figure 4 (c). The peak located at a binding energy of

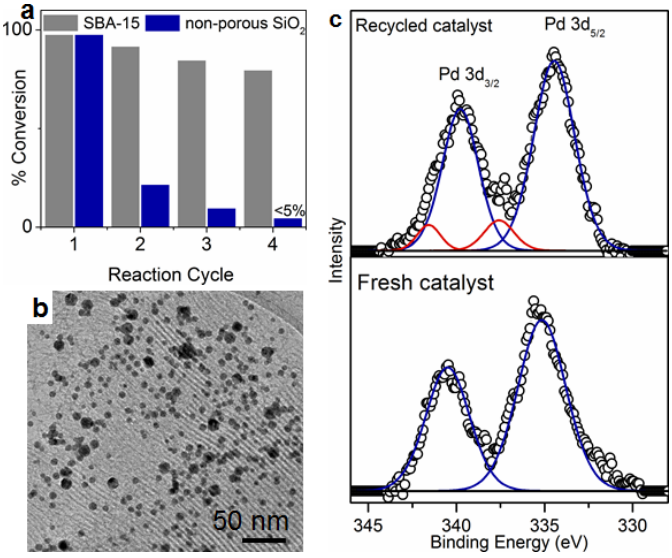


Figure 4. (a) Bar chart comparing yield after recycling SBA-15 and non-porous SiO_2 in Suzuki reaction. (b) TEM image of SBA-15 catalyst after reaction. (c) Pd 3d core level XPS of SBA-15 catalyst before and after 4 reaction cycles.

Please do not adjust margins

335 eV and 340 eV are assigned to the Pd $3d_{5/2}$ and $3d_{3/2}$ for Pd(0), respectively.[37] Analysis of the recycled catalyst shows mainly metallic Pd, with an additional low intensity peak corresponding to Pd(II) species at a binding energy of 337.6 eV, associated with PdO.[37] It is interesting to note that the binding energy of the Pd3d for the used catalyst shifts by 0.5 eV to a lower binding energy at 334.5 eV. This shift may be associated with changes in NP size and crystallinity of the alloys as observed by TEM.

Conclusions

Supercritical fluids are demonstrated as a simple and effective method of embedding pre-synthesized colloidal NPs with controlled size and composition, into ordered mesoporous SiO_2 support materials for catalysis. This approach can be useful for many catalytic and electrocatalytic applications of colloidal NPs. Incorporation of the NPs does not hinder their catalytic activity and the beneficial effective of the porous support for catalyst durability and recyclability is clearly demonstrated. SCFs and gas expanded liquids have potential for the preparation of heterogeneous catalysts. SCFs are commonly used for NP synthesis and size selective precipitation, with further possibility to combine these approaches with SCF-impregnation into porous support materials.

Acknowledgements

We would like to thank National University of Ireland for financial support…Other grants

Notes and reference

1. M. B. Gawande, A. Goswami, T. Asefa, H. Guo, A. V. Biradar, D.-L. Peng, R. Zboril and R. S. Varma, *Chem. Soc. Rev.*, 2015, **44**, 7540-7590.
2. A. K. Singh and Q. Xu, *ChemCatChem*, 2013, **5**, 652-676.
3. N. Pal and A. Bhaumik, *RSC Adv.*, 2015, **5**, 24363-24391.
4. A. Taguchi and F. Schuth, *Micropor. Mesopor. Mat.*, 2005, **77**, 1-45.
5. C. M. Yang, P. H. Liu, Y. F. Ho, C. Y. Chiu and K. J. Chao, *Chemistry of Materials*, 2003, **15**, 275-280.
6. M. J. Skaug, L. Wang, Y. Ding and D. K. Schwartz, *ACS Nano*, 2015, **9**, 2148-2156.
7. G. Collins, M. Blomker, M. Osaik, J. D. Holmes, M. Bredol and C. O'Dwyer, *Chem. Mater.*, 2013, **25**, 4312-4320.
8. J. Kim, J. E. Lee, J. Lee, J. H. Yu, B. C. Kim, K. An, Y. Hwang, C. H. Shin, J. G. Park, J. Kim and T. Hyeon, *J. Am. Chem. Soc.*, 2006, **128**, 688-689.
9. S. H. Joo, J. Y. Park, C.-K. Tsung, Y. Yamada, P. Yang and G. A. Somorjai, *Nat. Mater.*, 2009, **8**, 126-131.
10. R. Nafria, P. Ramirez de la Piscina, N. Homs, J. Ramon Morante, A. Cabot, U. Diaz and A. Corma, *J. Mater. Chem. A*, 2013, **1**, 14170-14176.
11. Y. Arai, T. Sako and Y. Takebayashi, *Supercritical fluids: molecular interactions, physical properties and new applications*, Springer Science & Business Media, 2013.
12. X. Zhang, S. Heinonen and E. Levanen, *Rsc Advances*, 2014, **4**, 61137-61152.
13. M. McHugh and V. Krukonis, *Supercritical fluid extraction: principles and practice*, Elsevier, 2013.
14. T. Hasell, C. D. Wood, R. Clowes, J. T. A. Jones, Y. Z. Khimyak, D. J. Adams and A. I. Cooper, *Chem. Mater.*, 2010, **22**, 557-564.
15. P. S. Shah, T. Hanrath, K. P. Johnston and B. A. Korgel, *J. Phys. Chem. B*, 2004, **108**, 9574-9587.
16. H. Zhang, J. M. Sun, D. Ma, X. H. Bao, A. Klein-Hoffmann, G. Weinberg, D. S. Su and R. Schlogl, *J. Am. Chem. Soc.*, 2004, **126**, 7440-7441.
17. R. E. Benfield, *J. Chem. Soc., Faraday Trans.*, 1992, **88**, 1107-1110.
18. S. Zhang, O. Metin, D. Su and S. Sun, *Angew. Chem. Int. Ed.*, 2013, **52**, 3681-3684.
19. G. X. Pei, X. Y. Liu, A. Wang, A. F. Lee, M. A. Isaacs, L. Li, X. Pan, X. Yang, X. Wang, Z. Tai, K. Wilson and T. Zhang, *ACS Catal.*, 2015, **5**, 3717-3725.
20. P. Aich, H. Wei, B. Basan, A. J. Kropf, N. M. Schweitzer, C. L. Marshall, J. T. Miller and R. Meyer, *J. Phys. Chem. C*, 2015, **119**, 18140-18148.
21. S. Gonzalez, K. M. Neyman, S. Shaikhutdinov, H.-J. Freund and F. Illas, *J. Phys. Chem. C*, 2007, **111**, 6852-6856.
22. A. K. Singh, Y.-H. Hwang and D.-P. Kim, *Npg Asia Materials*, 2015, **7**.
23. X. Zhao, R. Long, D. Liu, B. Luo and Y. Xiong, *J. Mater. Chem. A*, 2015, **3**, 9390-9394.
24. J. Yang, J. Yang and J. Y. Ying, *ACS Nano*, 2012, **6**, 9373-9382.
25. X. Lu, H.-Y. Tuan, J. Chen, Z.-Y. Li, B. A. Korgel and Y. Xia, *J. Am. Chem. Soc.*, 2007, **129**, 1733-1742.
26. Z. Yin, Y. Zhang, K. Chen, J. Li, W. Li, P. Tang, H. Zhao, Q. Zhu, X. Bao and D. Ma, *Sci. Rep.*, 2014, **4**, 4288.
27. Y. Kuwahara, M. Morita, T. Nagami, A. Tanaka, T. Iwanaga, K. Kumamaru, T. Sawada, M. Sasaki, M. Goto and M. Sato, *Japanese Journal of Applied Physics*, 2009, **48**.
28. Z. Nui and Y. Li, *Chem. Mater.*, 2014, **26**, 72-83.
29. S. Kotha, K. Lahiri and D. Kashinath, *Tetrahedron*, 2002, **58**, 9633-9695.
30. G. Collins, M. Schmidt, C. O'Dwyer, G. McGlacken and J. D. Holmes, *ACS Catalysis*, 2014, **4**, 3105-3111.
31. J.-S. Chen, A. N. Vasiliev, A. P. Panarello and J. G. Khinast, *J. Appl. Cat. A*, 2007, **325**, 76-86.
32. S. Sarina, H. Zhu, E. Jaatinen, Q. Xiao, H. Liu, J. Jia, C. Chen and J. Zhao, *J. Am. Chem. Soc.*, 2013, **135**, 5793-5801.
33. L. Feng, H. Chong, P. Li, J. Xiang, F. Fu, S. Yang, H. Yu, H. Sheng and M. Zhu, *J. Phys. Chem. C*, 2015, **119**, 11511-11515.
34. L. Zhang, A. Wang, J. T. Miller, X. Liu, X. Yang, W. Wang, L. Li, Y. Huang, C.-Y. Mou and T. Zhang, *ACS Catalysis*, 2014, **4**, 1546-1553.
35. G. Collins, M. Schmidt, C. O'Dwyer, J. D. Holmes and G. P. McGlacken, *Angew. Chem. Int. Ed.*, 2014, **53**, 4142-4145.
36. S. S. Soomro, F. L. Ansari, K. Chatziapostolou and K. Koehler, *J. Catal.*, 2010, **273**, 138-146.
37. G. Collins, M. Schmidt, G. P. McGlacken, C. O'Dwyer and J. D. Holmes, *J. Phys. Chem. C*, 2014, **118**, 6522-6530.

This journal is © The Royal Society of Chemistry 20xx

Please do not adjust margins